NJC

New Journal of Chemistry

A journal for new directions in chemistry

This article can be cited before page numbers have been issued, to do this please use: T. Geng, C. Hu, M. Liu, C. Zhang, H. Xu and X. Wang, *New J. Chem.*, 2020, DOI: 10.1039/D0NJ02912B.

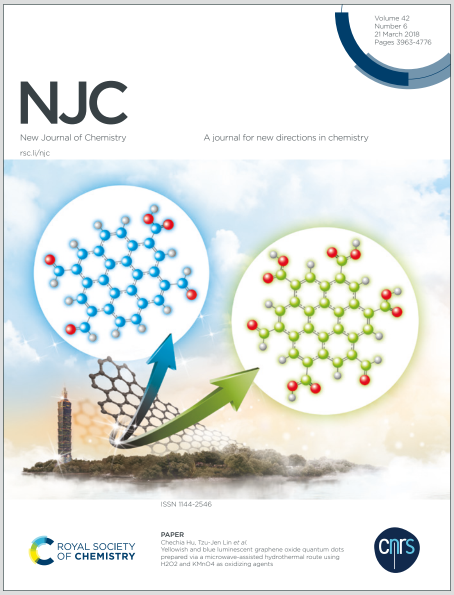

Volume 42
Number 6
21 March 2018
Pages 3963-4776

NJC
New Journal of Chemistry
A journal for new directions in chemistry
rsc.li/njc

ISSN 1144-2546

ROYAL SOCIETY OF CHEMISTRY

PAPER
Chechia Hu, Tzu-Jen Lin *et al.*
Yellowish and blue luminescent graphene oxide quantum dots prepared via a microwave-assisted hydrothermal route using H2O2 and KMnO4 as oxidizing agents

ROYAL SOCIETY OF CHEMISTRY

rsc.li/njc

New journal of chemistry

PAPER

View Article Online
DOI: 10.1039/D0NJ02912B

The influences of the structure of thiophene-based conjugated microporous polymers on the fluorescence sensing properties

Received 00th January 20xx,
Accepted 00th January 20xx

DOI: 10.1039/x0xx00000x

www.rsc.org/

Tong-Mou Geng*, Chen Hu, Min Liu, Can Zhang, Heng Xu, and Xie Wang

Abstract Three thiophene-based conjugated microporous polymers (CMPs: TTPTh, DBTh, and TBTh) were prepared by Sonogashira-Hagihara cross-coupling polymerization, and their structures were characterized by FTIR, ss ^{13}C NMR, and elemental analysis. The obtained TTPTh, DBTh, and TBTh have excellent thermal stability with decomposition temperature of 615, 298, and 290 °C and high porosity with BET surface area of 564.97, 416.99, and 521.30 $m^2\ g^{-1}$, respectively. The results reveal that the conjugation of the CMPs plays an essential role in determining fluorescence sensing performances. Because of perfect conjugation arising from a low volume of the building block or low degree of cross-linking, DBTh has high fluorescence sensing sensitivity to 2,4-dinitrophenol (DNP) and iodine with K_{sv} of 5.76×10^4 and 4.52×10^4 $L\ mol^{-1}$ and with LODs of 1.56×10^{-10} and 3.32×10^{-12} $mol\ L^{-1}$. To the best of our knowledge, the sensitivity to DNP and iodine of DBTh is the highest among all thiophene-based CMPs reported to date. Our study provides an essential understanding for the structure design of fluorescent sensors of CMPs.

1. Introduction

In the 21st century, people are attaching much importance to porous organic polymers (POPs) in view of the modular structure and optimization principles. So far, many kinds of POPs have been developed, including covalent organic framework (COFs),[1] polymer aromatic framework (PAFs),[2] covalent triazine-based frameworks (CTFs),[3] conjugated microporous polymers (CMPs),[4] hyper-crosslinked polymers (HCPs), and polymers of intrinsic microporosity (PIMs).[5] By changing the building unit, the performance of POPs can be optimized, with favorable control over the surface area, chemical stability, and fluorescence sensing properties. Therefore, POPs have excellent applications in various aspects, such as fluorescence probe,[4] drug delivery therapy,[6] storage,[7] adsorption,[8,9] separation,[10] gas separation and storage,[11,12] adsorbed liquid ions,[4] photoelectric effect,[13] catalysis,[14] and so on.

Recently, CMPs have been highly explored as an essential kind of POPs for their large specific surface area, excellent porosity, low skeleton density (light element), strong covalent bond, and extended π conjugated system.[15] Porous nature promotes the transmission of analytes and contact with action points on CMPs. The rigid skeleton structure avoids the quenching caused by the aggregation of fluorescent groups.[16] Moreover, they have excellent physicochemical stability. It could expect that these advantages described above enable them are more suitable for practical fluorescent sensing applications.[15]

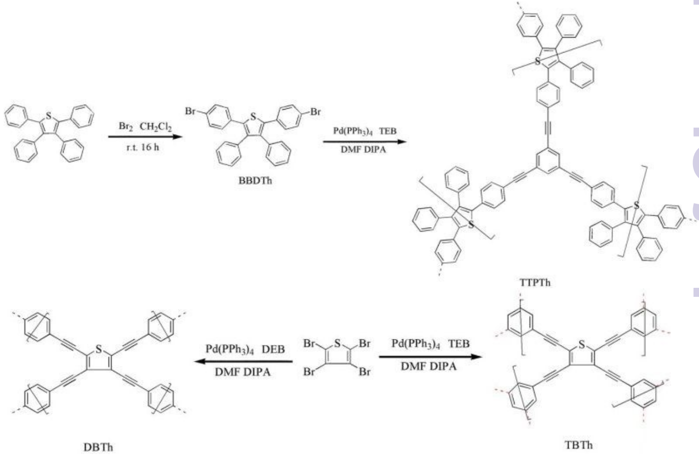

Scheme 1. Synthesis of BBDTh, TTPTh, DBTh, and TBTh.

The thiophene-containing CMPs are novel thiophene-based porous polymers, which have been studied by some material scientists and chemists. The excellent electrical, charge transport, redox, optical, and photoluminescence characteristics of thiophene-based CMPs have led to their a large variety of application in the fields of energy storage, electrocatalysis, electrochemical or bio-electrochemical sensors.[17-21] Although there are many reports on the properties of thiophene-based CMPs, there are only a few reports on their fluorescence sensing

---

AnHui Province Key Laboratory of Optoelectronic and Magnetism Functional Materials; School of Chemistry and Chemical Engineering, Anqing Normal University, Anqing 246011.

†Electronic Supplementary Informa(on (ESI) available: Synthesis of three CMPs, FT-IR, SS ^{13}C NMR, PXRD, TGA, UV-Vis, SEM, BET, and HOMO-LUMO energy levels of the CMPs, Effects of solvents, response time, DNP and I_2 on fluorescent spectra. See DOI:10.1039/x0xx00000x

DOI: 10.1039/D0NJ02912B

properties. Furthermore, the sensitivity of these thiophene-based CMPs needs to be further improved.[22-26]

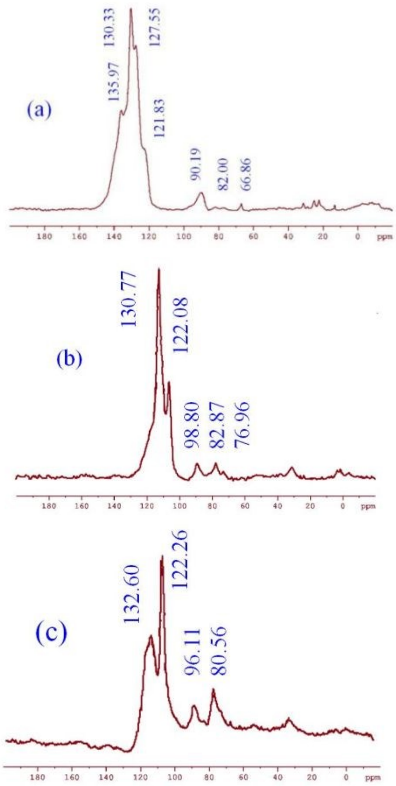

Fig. 1. ss ^{13}C NMR spectra of TTPTh, DBTh, and TBTh.

2,4-dinitrophenol (DNP) is one of the nitro-aromatic compounds (NACs), which acts as the crude materials for industries of explosives, fireworks, matches, rocket fuels, dyes, leathers, and medicines. Because of its wide applications, it can be easily released into soil and groundwater, and even if it contacts them occasionally, it may irritate the eyes and skin and even damage the respiratory system.[27,28] Furthermore, because it possesses a strong ability to withdraw electron, DNP is difficult to degrade into nontoxic compounds.[27] Hence, it is important to develop a simple, rapid, and selective analytical method for DNP detection. DNP, similar to most NACs, can act as suitable fluorescent quenchers owing to the presence of electron-deficient -NO_2 groups, which makes sensors based on fluorescence quenching to be the most effective tools for the detection of DNP.[29] Nevertheless, to the best of our knowledge, there are no CMPs to date for fluorescence detection of DNP.

Molecular iodine shows a brown color and becomes toxic, which can be emitted when iodine-containing substances under exposure to light. Therefore, it is necessary to monitor the content of molecular iodine in iodine-containing drugs during their synthesis and long-term storage. At present, there are various analytical methods for the determination of iodine content in organic substances, including colorimetry, spectrophotometry, electrochemical method, chromatography spectrometry, ion chromatography, fluorescence method, and so on. However, it is still a time-consuming and intricate task for quantitative determination. This is because of the volatility of iodine, its multivalency, and the ease of redox reactions with the components of the substance analyzed. Among the above methods, fluorescence spectrometry is relatively simple, sensitive, and can meet the requirements of rapid analysis of iodine.[30] Lately, our group have developed fluorescence detection for molecular iodine by CMPs and achieved good results.[31,32] However, the sensitivity of thiophene-based CMPs to iodine needs to be improved.[33]

In this manuscript, we present three thiophene containing CMPs with different cross-linking degree and size building blocks to discuss further the effect of the molecular structure on the fluorescence sensing performances of NACs and iodine (Scheme 1). It is exciting to note that the conjugation of the CMPs has an essential effect on the fluorescence sensing performance. The CMPs with small size building blocks or a low degree of cross-linking demonstrate a high quenching coefficient (K_{sv}). It can be said that our findings provide a basic understanding of structural design of CMP chemsensors.

2. Results and discussion

2.1. Characterization, morphology analysis, and pore performance

2.1.1. Characterization and morphology analysis

Scheme 1 shows the synthetic routes of the three CMPs (TTPTh, DBTh, and TBTh) and building block 2,5-bis(4-bromophenyl)-3,4-diphenylthiophene (BBDTh). The formation of the BBDTh was confirmed using a range of analytical techniques (Fig. S1 and S2). The three CMPs were prepared by Sonogashira-Hagihara cross-coupling polymerization reaction with yields of 62.72%, 81.57%, and 73.15%, respectively. Their chemical structure were corroborated by solid-state ^{13}C NMR spectra (ss ^{13}C NMR), Fourier Transform Infrared (FT-IR), and elemental analyses (EA). The strong stretching vibration of C–Br at 1477/1481 cm^{-1} nearly disappeared compared with C–C, indicating the almost complete conversion of C–Br (Fig. S3).[34,35] The vibration peaks of terminal C≡C triple bond (arising from unreacted end groups) at about 3298 cm^{-1} were very weak, while the peaks of bissubstituted acetylenes cut near 2202/2197 cm^{-1} appeared except for TTPTh, which may be due to the large group of monomer BBDTh.[36,37] The peaks at 1636/1657/1646, 1564/1504/1576, and 1475/1504/1412 cm^{-1} were C=C stretching vibration in the skeleton of the phenyl ring. The absorption peaks at 1475/1462/1412 and 1384/1396/1317 cm^{-1} come of the stretching vibration of C=C and C–C in the thiophene unit. The signals at 1289/1274/1240 cm^{-1}, 1072/1171/1119 cm^{-1} result from the stretching vibration of C–S–C. In addition, the peaks at 834/834/882 cm^{-1} are the deformation of C–S.[38] These characterization data indicate that the three CMPs have been synthesized. As illustrated in ss ^{13}C NMR (Fig. 1), for TTPTh, the peak observed at 135.97 ppm belongs to substituted aromatic carbon bound to thiophene. The peak of 127.55 ppm is aromatic substituted aromatic carbon, which is connected with thiophene. The peak at 130.33 ppm is

View Article Online
DOI: 10.1039/D0NJ02912B

attributed to the carbon atoms on benzene. For DBTh and TBTh, the peaks at around 122 ppm are part of aromatic carbon on thiophene. The peaks at 130.77/132.60 ppm are attributed to the carbon atoms on benzene. For the three CMPs, the peaks observed at 90.19/98.80/96.11 ppm, 82.00/82.87/80.56 ppm, and 76.96/76.96 ppm belong to the carbon on the alkynyl group.[34,39] The results of elemental analysis show that the H, N, and H contents of the three CMPs are basically consistent with the theoretical calculation (see S1 and S2).

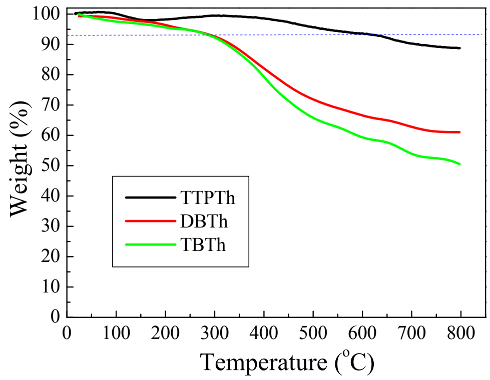

Fig. 2. TGA analysis data of CMPs. (a) TTPTh, DBTh, and (c) TBTh. Data collected by heating at 10 °C min^{-1} under a nitrogen atmosphere.

To the naked eye, all the three CMPs appear to be brown powder. They are insoluble in organic solvents and water. They are chemically stable to acids, bases, and ordinary solvents. Further analysis of these CMPs by TGA showed that they were stable at 615°C, 298°C, and 290°C, respectively (Fig 2).[40]

Powder X-ray diffraction patterns (PXRD) indicated the amorphous structure of the three CMPs (Fig. S4). Scanning electron microscopy (SEM) showed that TTPTh and TBTh are spherical structures joined together, while DBTh is a fiber-like structure (Fig. S5).

2.1.2. Pore performance of the obtained materials

The nitrogen adsorption method was used to analyze the CMP networks, and the desorption curves were located above the adsorption curve (Fig. 3a). TTPTh showed obvious hysteresis type I gas adsorption isotherm, DBTh and TBTh showed obvious hysteresis type II gas adsorption isotherms classified by IUPAC. The significant hysteresis is most likely due to the mesoporous structure of the samples[41] and the presence of intergranular spaces. BET surface areas and pore performances of the three CMPs were listed in Table 1.TTPTh, DBTh, and TBTh have large specific surface areas up to 564.97, 416.99, 521.30 m^2 g^{-1} and high pore volume with 0.4121, 0.2905, 0.5560 cm^3 g^{-1}, respectively. To calculate the microporosity, we have calculated the ratio of $V_{0.1}/V_{tot}$, which are 0.4596, 0.4689, and 0.1888 for TTPTh, DBTh, and TBTh, respectively, indicating that TTPTh and DBTh belong to microporous materials, whereas there are mesopores in the TBTh material.[41,42] Non-local density functional theory (NL-DFT) slit pore geometry model has successfully calculated the pore size distribution and relative pore size (Fig. 3b). The apertures of TTPTh, DBTh, and TBTh are estimated at 1.22, 2.79, and 5.69 nm, respectively.

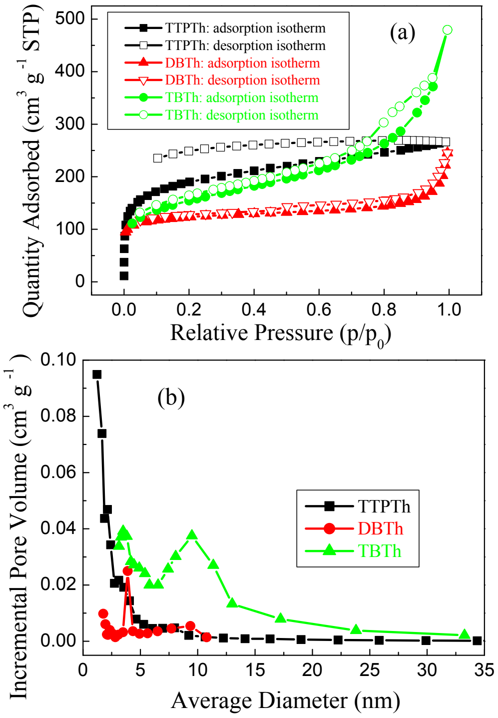

Fig. 3. (a) Nitrogen adsorption–desorption isotherms at 77 K. (b) Pore size distribution based on non-local density functional theory (NLDFT) calculation.

Table 1. Pore and surface properties of TTPTh, DBTh, and TBTh.

CMPs	S_{BET}^{a} (m^2 g^{-1})	S_{Lang} (m^2 g^{-1})	V_{total} (tpv)^b (cm^3 g^{-1})	V_{micro}^{c} (cm^3 g^{-1})	V_{micro}/V_{total}	S_{micro}^{c} (m^2 g^{-1})
TTPTh	564.97	684.86	0.4121	0.1894	0.4596	185.50
DBTh	416.99	560.41	0.2905	0.1362	0.4689	292.70
TBTh	521.30	799.57	0.5560	0.1050	0.1888	210.41

a Specific surface area calculated from the adsorption branch of the nitrogen isotherm using the BET method in the relative pressure (p/p_0) range from 0.01 to 0.10.

b Total pore volume is obtained from BET data up to p/p_0=0.97 and is defined as the sum of micropore volume and volumes of larger pores.

c Micropore volume calculated from nitrogen adsorption isotherm using the t-plot method.

2.2. Fluorescent sensing property for NACs and I_2

2.2.1. Fluorescent property and response time

The electronic absorption properties of monomers and CMPs were observed by UV-Vis spectroscopy. TTPTh and BBDTh showed broad absorption peaks of 228-430 nm and 268-322 nm, while other building block 1,3,5-triethynylbenzene (TEB) showed a narrow absorption peak at 231 nm. The peaks have moved 89 and 127 nm to the right. The peaks of DBTh and TBTh are about 465-468 and 381-415 nm, which have red-shifts 117, 173 and 64, 150 nm compared with the corresponding monomers TBrTh, 1,4-diethynylbenzene (DEB), and TEB. These

View Article Online
DOI: 10.1039/D0NJ03913B

results indicated the existence of π-conjugated CMPs (Fig. S6).[43] The absorption peaks of TTPTh, DBTh, and TBTh were at 358, 434, and 381 nm, respectively, indicating that DBTh has the best conjugation performance among the three CMPs. It is most likely because DBTh's building unit volume is smaller than TTPTh's, but the cross-linking density of DBTh is lower than that of TBTh.

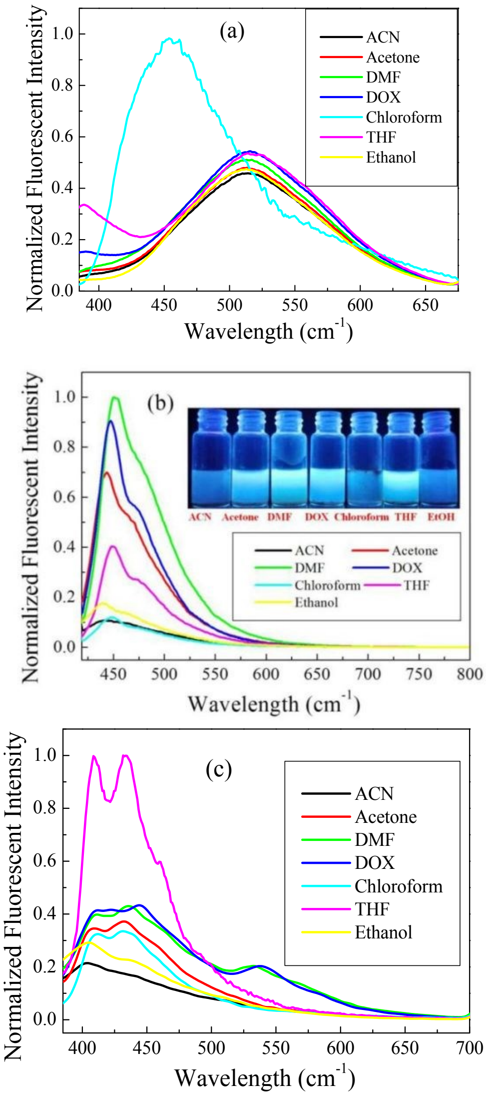

Fig. 4. Fluorescent spectra of (a) TTPTh, (b) DBTh, and (c) TBTh in various solvents (1.0 mg mL^{-1}, λex=360, 410 and 362 nm), Insert of (b): Photographs of DBTh suspensions in different solvents under UV irradiation at 365 nm.

The solid-state fluorescence spectra of the three CMPs and the corresponding monomers as well as model compound tetraphenylthiophene (TPTh) at room temperature were shown in Fig. S7 and S8, which showed that when excited at 478, 445, and 301 nm, the emission peaks of TTPTh, DBTh, and TBTh are at 715, 680, and 569 nm, respectively. The emission peaks of TEB, DEB, BBDTh, and TPTh are located at 565, 529, 513, and 541 nm, respectively. Compared with monomers, the maximum fluorescence emission peaks of the three CMPs showed red-shift, indicating that the as-synthesized CMPs had high degrees of polymerization. Moreover, The presented emission spectra in Fig. S8 are extremely small because of the low conjugation effect for the monomers and the fluorescence quenching effect caused by aggregation.[36,44-46]

TTPTh, DBTh, and TBTh were dispersed in acetone, acetonitrile (ACN), dimethylformamide (DMF), 1,4-dioxane (DOX), ethanol (EtOH), chloroform, and tetrahydrofuran (THF) to investigate the potential applications as fluorescent sensors for the detection of NACs and I_2.[47] As shown in Fig. 4, TTPTh, DBTh, and TBTh emitted strong fluorescence when they were dispersed in trichloromethane, DMF and THF, respectively. Under UV irradiation at 365 nm, only DBTh emitted bright cyan fluorescence in ACN, DMF, DOX, and THF suspension (Fig. 4b Insert). The corresponding CIE coordinate of DBTh was found to be (0.1662, 0.1848), (0.2701, 0.5686), (0.2237, 0.5132), and (0.239, 0.4834) excited by 410 nm, all within the green-light region in the chromaticity graph except for in ACN (Fig. S9).[45,48,49] So we chose chloroform, DMF, and THF as the solvents for severally dispersing TTPTh, DBTh, and TBTh to conduct the sensing experiments through fluorescence quenching.

The fluorescence intensity of the dispersions for the three CMPs with time before and after adding into DNP or I_2 was shown in Fig. S10 and Fig. S11. As expected, when different concentrations of DNP and I_2 were added into TTPTh-chloroform, DBTh-DMF, and TBTh-THF dispersion, the fluorescence intensity of TTPTh, DBTh, and TBTh instantaneously decreased in the 20s, indicating that the three CMPs have ultrafast fluorescence response rates for DNP and I_2. It demonstrates the effective "real-time" detection of DNP and I_2 by the three CMPs.[50–53]

2.2.2. Sensitivity to DNP and iodine

The sensitivity (slopes of linear response ranges and limit of detection (LOD)) of the three sensor systems were measured under optimized experimental conditions. DNP solutions at different concentrations of chloroform, DMF, and THF were added into the suspensions of TTPTh, DBTh, and TBTh for fluorescence quenching titration, respectively. As shown in Fig. 5a-d, their fluorescence intensity decreased with increasing DNP concentration over a wide concentration ranges. The relative fluorescence intensities (I_0/I) were linear with the DNP concentration at low concentration (Fig. 5e). The quenching efficiencies of the DNP were determined by Stern–Volmer equation, $I_0/I=1+K_{sv}[\text{analyte}]$,[54] where I_0 and I are the fluorescence intensity when the analyte is not added and the analyte is added. K_{sv} is the Stern-Volmer quenching constant. The K_{sv} values of TTPTh, DBTh, and TBTh were 1.10×10^4, 5.76×10^4, and 9.59×10^3 L mol^{-1}, respectively. LOD is calculated using the formula: 3S/ρ (S is the standard deviation of background noise from the calibration curve, ρ is the slope of the linear relationship).[22,54] The LODs of TTPTh, DBTh, and TBTh for DNP are estimated to be very low with 5.47×10^{-10}, 1.56×10^{-10}, and 9.38×10^{-9} mol L^{-1}, respectively. The sensitivity of DBTh is higher than that of TTPTh and TBTh. We conjecture that the building block (TBrTh) of DBTh is smaller to that (BBDTh) of TTPTh, the degree cross-linking of DBTh is smaller than that of

View Article Online
DOI: 10.1039/D0NJ02912B

TBTh. Hence, the conjugation of DBTh is considerable more than that of TTPTh and TBTh. We continued to investigate the fluorescence sensing of iodine by three CMPs. The results show that their sensitivity to iodine is consistent with DNP (Fig. S12 and Table S1).

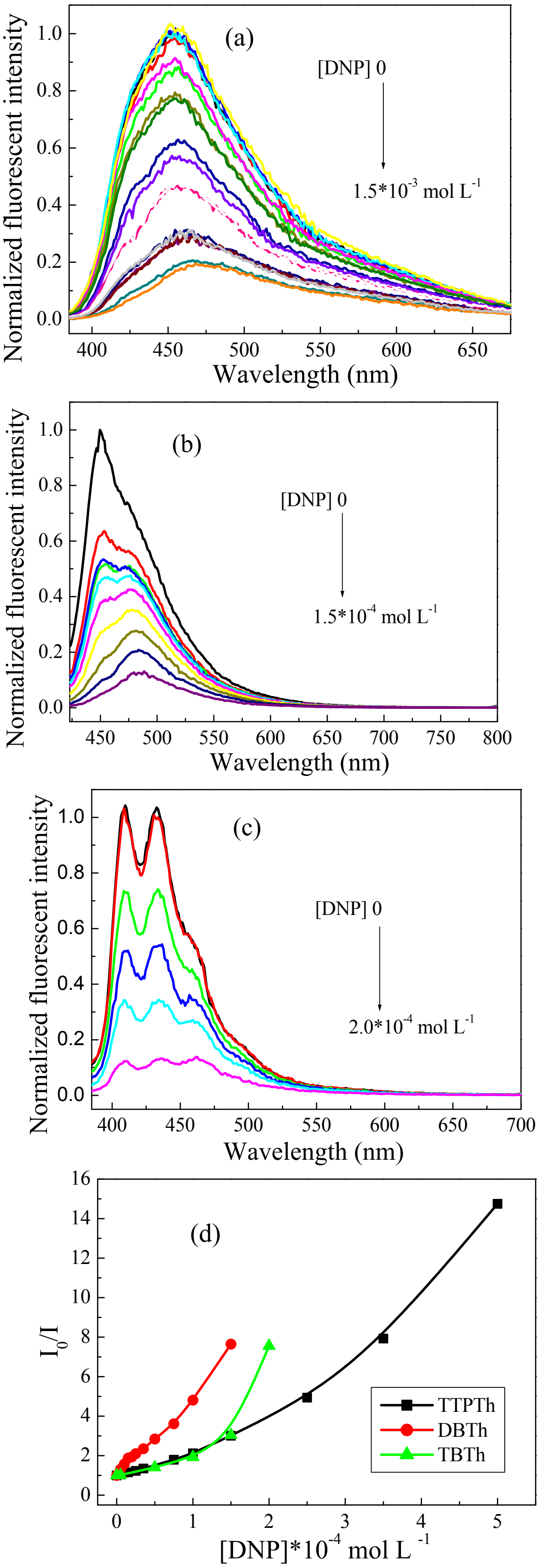

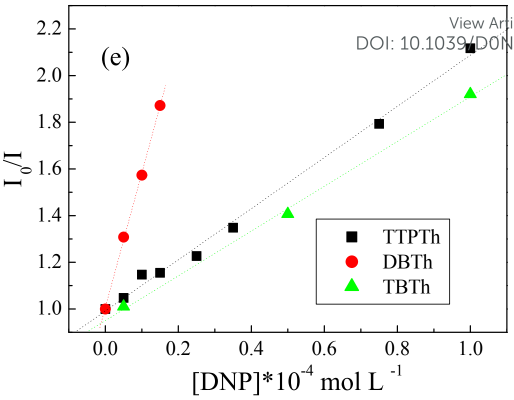

Fig. 5. The changes of fluorescent spectra of (a) TTPTh, (b) DBTh, and (c) TBTh severally in chloroform, DMF, and THF with the fluorescence intensity I_0/I of DNP; (d) I_0/I of the TTPTh, DBTh, and TBTh in suspensions upon addition of various concentrations of DNP; (e) Stern–Volmer plots of TTPTh, DBTh, and TBTh with various concentrations of DNP (1.0 mg mL^{-1}, excited at 360, 410, and 362 nm).

The property of the three sensors for detecting DNP and I_2 was compared with that of reported in the literatures, as shown in Table S2-S4. It should be noted that no reports of thiophene-based CMPs used to detect DNP have been found. Moreover, compared with other reported thiophene-based CMPs, TTPTh, DBTh, and TBTh sensor systems have the highest sensitivity to iodine (Table S2).[33] As shown in Table S3, there are many detection methods that were employed, including solid-phase microextraction coupled to gas chromatography-mass spectrometry, electrochemical sensors, solid-phase extraction followed by ultrahigh-pressure liquid chromatography–QTRAP®MS, and fluorescence sensors. We summarized the work of fluorescence sensing to I_2. The LOD of DBTh is 1.56×10^{-10} mol L^{-1}, which is better than other reported methods (Table S4). The sensing mechanism of all systems in Table S4 is based on fluorescence quenching, which may be due to the electron transfer from the CMPs to the I_2, thus forming the electron transfer complexes. Although the sensitivities of the three CMPs are slightly lower than that reported other types of CMPs,[31,32] the sensitivity of TTPTh, DBTh, and TBTh sensors are higher than that of other thiophene-based CMPs.[33]

NACs, including nitrobenzene (NB), o-NP, 2,4-dinitrotoluene (DNT), p-dinitrobenzene (p-DNB), picric acid (PA), m-dinitrobenzene (m-DNB), 4-nitrotoluene (p-NT), DNP, 4-nitrophenol (p-NP), 3-nitrophenol (m-NP), and nitrobenzene (NB), as well as iodine were selected as analytes for chemical sensing studies. The selectivity of DBTh to DNP detection was studied by adding 1.5×10^{-4} mol L^{-1} of NACs and I_2 into the DMF suspension of DBTh, and the emission intensity remarkably decreased for only I_2 and PA. The selectivity of TBTh to DNP detection was studied by added 2.0×10^{-4} mol L^{-1} of DNP into THF suspension of TBTh. The emission intensity decreased for only DNP, p-DNB, and o-NP (Fig. 6, red bar). The results suggested that DBTh and TBTh have selectivity for DNP over other NACs.[44,55,56]

We conducted the competitive tests of DBTh and TBTh for DNP detection. First, 1.5×10^{-4} and 2.0×10^{-4} mol L^{-1} DNP was

View Article Online
DOI: 10.1039/D0NJ02912B

added to the colloidal solution of DBTh and TBTh (polymer concentration was 1.0 mg mL^{-1}), then other NACs or I_2 of the same concentration was added to DBTh and TBTh, respectively. The results were showed that the sensing of the DNP by DBTh was hardly affected by NACs except for I_2 and PA, and by TBTh except for p-DNB, o-NP (Fig. 6, green bar). The experiments also show that both DBTh and TBTh have selectivity for NACs.[22,23,57]

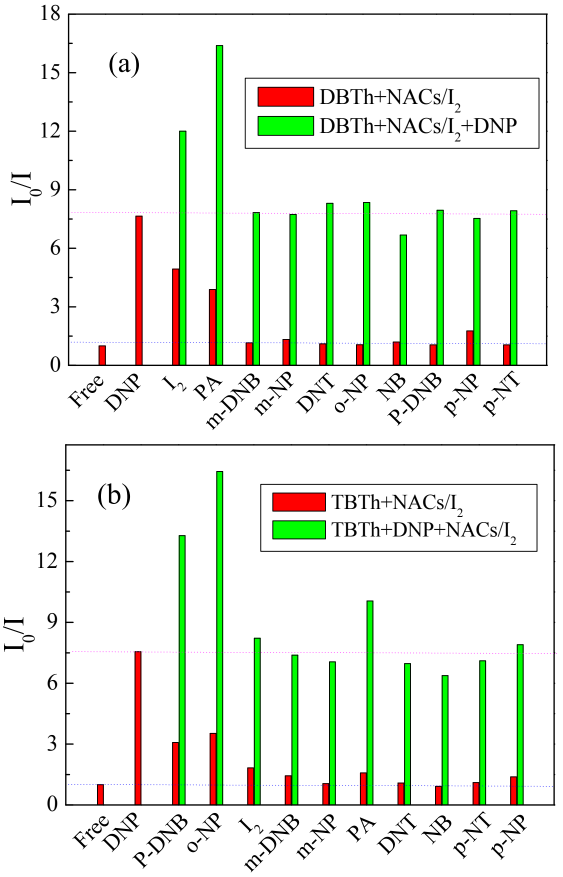

Fig. 6. Selectivity and competitiveness of (a) DBTh, and (b) TBTh in DMF and THF ([DNP]= 1.5×10^{-4} and 2.0×10^{-4} mol L^{-1}, λex = 410 and 362 nm). The red bars represent the relative fluorescent intensity of CMPs in the presence of the competition NACs, and the green bars represent the relative fluorescent intensity upon the addition of DNP to the above solution.

2.2.3. The mechanism of fluorescent sensing to NACs and I_2

To investigate the fluorescence sensing mechanism, the absorption spectra of NACs and I_2, as well as the fluorescence spectra of the three CMPs were determined (Fig. S13). The absorption spectrum of the DNP overlaps with the emission of TBTh, while the absorption of DNP has almost no spectral overlap with the emission of TTPTh and DBTh. On the other hand, both TTPTh and TBTh emission and I_2 absorption have spectral overlap, while DBTh emission and I_2 absorption have no spectral overlap. It fully proves that fluorescent quenching of TTPTh and DBTh by DNP belongs to the electron transfer mechanism, while that of TBTh by DNP is part of the photoinduced electron transfer mechanism. And it can also prove that fluorescent quenching of DBTh and TBTh by I_2 belongs to the electron transfer mechanism, whereas that of TTPTh by I_2 is part of the photoinduced electron transfer mechanism.[46,58–60]

The chemical sensing phenomenon depends on the energy levels of the lowest unoccupied molecular orbitals (LUMOs) of the NACs, I_2, and these three CMPs (Fig. S14 and Table S5). The calculated LUMO energy levels of DNP (-3.320 eV) and I_2 (-4.988 eV) are far lower than that of TTPTh (-1.726 eV), DBTh (-1.255 eV), and TBTh (-2.063 eV), thus providing a powerful driving force for photoinduced electron transfer.[50,55]

From Fig. 5d and Fig. S12d, these curves are bent upward, indicating that there is both a static quenching process and a dynamic quenching process.[56,61,62]

2.2.4. Fluorescence stability experiment

Taking DBTh as an example, the fluorescence stability of the CMPs was investigated. DBTh solid powder was baked in the air at 50°C, 100°C, 150°C, and 200°C for 30 min, respectively, after cooled to room temperature and then dispersed in DMF (1.0 mg mL^{-1}). Until 100℃ DBTh is still very stable and the fluorescence spectrum is almost unchanged. As the temperature increases further, the fluorescence emission peak gradually decreased without red-shift (Fig. S15).[37,63,64]

2.2.5. Practical application of DBTh sensor to sand sample

To further investigate the practical application of the three CMPs as chemosensors for DNP and I_2, we take DBTh as an example to carry out the experimental study. DNP (0.125 or 0.250 μmol), 5.0 g of naturally dried sand samples, and 0.125 g of water (2.5 wt% by weight of sand) were mixed. The mixture was extracted with DMF, ultrasound for 30 min, centrifuged for 10 min at 10,000 rpm, and the volume was fixed with a 25 mL volumetric flask.[65] The 25 mg of DBTh was added into the volumetric flask. Then the dispersions were determined with fluorescence spectra. It was found that DNP were 0.122 and 0.246 μmol for each 5 g sand, whose spiked recoveries were 97.6% and 98.4% of the amount added, relative standard deviations (RSD) were ±4.28% and ±3.85%, respectively (Fig. S16, Table S6). As in the experiments of sensing to DNP, it was found that when 0.025 and 0.05 μmol of iodine were added for each 5 g sand, whose spiked recoveries were 93.6% and 93.5% of the amount added, RSDs were ±3.94% and ±3.53%, respectively (Fig. S17, Table S7). Therefore, the DBTh as a chemosensor can effectively detect the contents of DNP and I_2 in sand.[37,65]

3. Conclusion

The thiophene-based conjugated microporous polymers are important conjugated microporous polymers, but they are rarely used in fluorescence sensing and are low sensitive. In this study, the three thiophene-based CMPs with different volume of building blocks and degree of cross-linking were devised and prepared. The effects of molecular structures of the three CMPs on the fluorescence sensing properties to NACs and iodine were studied. As a result, the conjugation of the CMPs plays an

View Article Online
DOI: 10.1039/D0NJ02912B

essential role in determining fluorescence sensing properties. Because of excellent conjugated properties arising from a low volume of building blocks and low degree of cross-linking, DBTh has high fluorescence sensing sensitivity to DNP and iodine with K_{sv} of 5.76×10^{4} and 4.52×10^{4} L mol^{-1} and with LODs of 1.56×10^{-10} and 3.32×10^{-12} mol L^{-1}.

Acknowledgements

This work was supported by Natural Science Foundation of Anhui Education Department (under Grant No. KJ2018A0319 and KJ2019A0558).

There is no conflict of interest.

References

1 Y.P. Song, Q. Sun, B. Aguila, S.Q. Ma, Covalent organic frameworks: opportunities of covalent organic frameworks for advanced applications, Adv. Sci. 6 (2019) 1801410.

2 Y. Yuan, G. Zhu Porous, aromatic frameworks as a platform for multifunctional, applications, ACS central. Sci. 5 (2019) 409–418.

3 P. Kuhn, M. Antonietti, A. Thomas Covalent triazine-based frameworks prepared by ionothermal synthesis, Angew. Chem. Int. Ed. 47 (2008) 3450–3453.

4 L. Xiang, Y. Zhu, S. Gu, D. Chen, X. Fu, Y. Zhang, G. Yu, C. Pan, Y. Hu A luminescent hypercrosslinked conjugated microporous polymer for efficient removal and detection of mercury ions, Macromol. Rapid. Comm. 36 (2015) 1566–1571.

5 G. Cheng, B. Bonillo, R.S. Sprick, D.J. Adams, T. Hasell, A.I. Cooper Conjugated polymers of intrinsic microporosity (C-PIMs), Adv. Funct. Mater. 24 (2014) 5219–5224.

6 L.Y Bai, W.Q. Lim, A. Jana, Z. Luo, H.J.P. Tham, L.Z. Zhao, Y.L. Zhao, Nanoscale covalent organic frameworks as smart carriers for drug delivery, Chem. Commun. 22 (2016) 4128–4131.

7 F. Xu, S. Yang, X. Chen, Q. Liu, H. Li, H. Wang, B. Wei, D. JiangEnergy-storage covalent organic frameworks: improving performance via engineering polysulfide chains on walls, Chem. Sci. 10 (2019) 6001–6006.

8 B. Li, Y. Zhang, R. Krishna, K. Yao, Y. Han, Z. Wu, D. Ma, Z. Shi, T. Pham, B. Space, J. Liu, P.K. Thallapally, J. Liu, M. Chrzanowski, S. Ma, Introduction of π-complexation into porous aromatic framework for highly selective adsorption of ethylene over ethane, J. Am. Chem. Soc. 136 (2014) 8654–8660.

9 W. Xie, S.R. Zhang, Y.H. Xu, D.L. Jiang, Iodine capture in porous organic polymers and metal–organic frameworks materials, Mater. Horiz. 8 (2019) 1571–1595.

10 Q. Song, S. Cao, R.H. Pritchard, H. Qiblawey, E.M. Terentjev, A.K. Cheetham, E. Sivaniah, Nanofiller-tuned microporous polymer molecular sieves for energy and environmental processes, J. Mater. Chem. A 4 (2016) 270–279.

11 S.C. Fraga, M. Monteleone, M. Lan, E. Esposito, A. Fuoco, L. Giorno, K. Pilnáek, K. Friess, M. Carta, N.B. McKeown, P. Izák, Z. Petrusová, J.G. Crespo, C. Brazinha, J.C. Jansen, A novel time lag method for the analysis of mixed gas diffusion in polymeric membranes by on-line mass spectrometry: Method development and validation, J. Membrane. Sci. 561 (2018) 39–58.

12 F.A. Nugroho, C. Xu, N. Hedin, C. Langhammer UV–visible and plasmonic nanospectroscopy of the CO_2 adsorption energetics in a microporous polymer, Anal. chem. 87 (2015) 10161–10165.

13 S.Y. Ding, W. Wang, Covalent organic frameworks (COFs): from design to applications, Chem. Soc. Rev. 42 (2013) 548–568.

14 W. Gong, Q. Wu, G. Jiang, G. Li, Ultrafine silver nanoparticles supported on a covalent carbazole framework as high-efficiency nanocatalysts for nitrophenol reduction, J. Mater. Chem. A 7 (2019) 13449–13454.

15 S.H. Xiong, X. Tang, C.Y. Pan, L. Li, J.T. Tang, G.P. Yu, Carbazole-bearing porous organic polymers with a mulberry-like morphology for efficient iodine capture, ACS. Appl. Mater. Inter. 30 (2019) 27335–27342.

16 Y.H. Xu, S.B. Jin, H. Xu, A. Nagai, D.L. Jiang, Conjugated microporous polymers: design, synthesis and application, Chem. Soc. Rev. 42 (2013) 8012–8031.

17 C.J. Sun, P.F. Wang, H. Wang, B.H. Han, All-thiophene-based conjugated porous organic polymers, Polym. Chem. 7 (2016) 5031–5038.

18 F. Piron, P. Leriche, G. Mabon, I. Grosu, J. Roncali, Electropolymerization of three–dimensional π–conjugated system based on 3,4–ethylenedioxythiophene (EDOT), Electrochem. Commun. 10 (2008) 1427–1430.

19 L.Q. Ouyang, C.C. Kuo, B. Farrell, S. Pathak, B. Wei, J. Qu, D.C. Martin, Poly[3,4-ethylene dioxythiophene (EDOT)-co-1,3,5-tri[2-(3,4-ethylene dioxythienyl)]-benzene (EPh)] copolymers (PEDOT-co-EPh): optical, electrochemical and mechanical properties, J. Mater. Chem. B 3 (2015) 5010–5020.

20 S.L. Bai, Q. Hu, Q. Zeng, M. Wang, L.S. Wang, Variations in surface morphologies, properties, and electrochemical responses to nitro-analyte by controlled electropolymerization of thiophene derivatives, ACS. Appl. Mater. Inter. 10 (2018) 11319–11327.

21 A.P. Cando, G. Brunklaus, U. Scherf, Thiophene-based microporous polymer networks via chemical or electrochemical oxidative coupling, Macromolecules 48 (2015) 6816–6824.

22 T.M. Geng, W.Y. Zhang, Z.M. Zhu, G.F. Chen, L.Z. Ma, S.N. Ye, Q.Y. Niu A covalent triazine-based framework from tetraphenylthiophene and 2,4,6-trichloro-1,3,5-triazine motifs for sensing o-nitrophenol and effective I_2 uptake, Polym. Chem. 9 (2018) 777–784.

23 T.M. Geng, Z.M. Zhu, X. Wang, H.Y. Xia, Y. Wang, D.K. Li, Poly{tris[4-(2-thienyl)phenyl]amine} fluorescent conjugated microporous polymer for selectively sensing picric acid, Sensor. Actuat. B-Chem. 244 (2017) 334–343.

24 F. Wei, X.Y. Cai, J.Q. Nie, F.Y. Wang, C.F. Lu, G.C. Yang, Z.X. Chen, C. Ma and Y.X. Zhang, A 1,2,3-triazolyl based conjugated microporous polymer for sensitive detection of p-nitroaniline and Au nanoparticles immobilization, Polym. Chem. 27 (2018) 3832–3839.

25 Y.S. Kochergin, D. Schwarz, A. Acharjya, A. Ichangi, R. Kulkarni, P. Eliáová, J. Vacek, J. Schmidt, A. Thomas, M.J. Bojdys, Exploring the “Goldilocks Zone” of semiconducting polymer photocatalysts by donor–acceptor interactions, Angew. Chem. Int. Ed. 57 (2018) 14188–14192.

26 M.J. Wu, Y. Han, B. Wang, Y. Yuan, C.F. Xing, Y.L. Chen, Heteroacene-based conjugated microporous polymers as fluorescent sensors and effective antimicrobial carriers, ACS Appl. Bio. Mater. 1 (2018) 473–479.

27 M. Fang, F. Lei, J. Zhou, Y.N. Wu, Z.Y. Gong, Rapid, simple and selective determination of 2,4-dinitrophenol by molecularly imprinted spin column extraction coupled with fluorescence detection. Chinese Chem. Lett. 25 (2014) 1492–1494.

28 Y. Liu, L.H. Zhu, Y.Y. Zhang, H.Q. Tang, Electrochemical sensoring of 2,4-dinitrophenol by using composites of graphene oxide with surface molecular imprinted polymer, Sensor. Actuat. B-Chem. 171–172 (2012) 1151–1158.

29 X.Y. Wan, F.L. Jiang, C.P. Liu, K. Zhou, L. Chen, Y.L. Gai, Y. Yang, M.C. Hong, Rapid and discriminative detection of nitro aromatic compounds with high sensitivity by two zinc MOFs synthesized through temperature-modulated method, J. Mater. Chem. A, 2015, 3, 22369–22376.

30 N.A. Gavrilenkoa, D.A. Fedan, N.V. Saranchina, M.A. Gavrilenko, Solid phase colorimetric determination of iodine in food grade salt using polymethacrylate matrix, Food Chem. 280 (2019) 15–19.

31 T.M. Geng, C. Zhang, G.F. Chen, L.Z. Ma, W.Y. Zhang, H.Y. Xia, Synthesis of tetraphenylethylene-based fluorescent conjugated microporous polymers for fluorescent sensing and adsorbing iodine, Micropor. Mesopor. Mat. 284 (2019) 468–475.

32 T.M.Geng, C. Zhang, C. Hu, M.Liu, Y.T. Fei, H.Y. Xia, Synthesis of 1,6-disubstituted pyrene-based conjugated microporous polymers for reversible adsorption and fluorescence sensing of iodine, New J. Chem. 44 (2020) 2312-2320.

33 T.M. Geng, L.Z. Ma, G.F. Chen, C. Zhang, W.Y. Zhang, H.Y. Xia, H. Zhu. Poly[1,3,6,8-tetra(2-thiophenyl)pyrene] and poly[1,3,6,8-tetra(3-thiophenyl)pyrene] conjugated microporous polymers for reversible adsorbing and fluorescent sensing iodine, J. Polym. Res. 26 (2019) 113-122.

34 H.G. Cha, C.W. Kim, S.W. Kang, B.K. Kim, Y.S. Kang, Preparation and characterization of the magnetic fluid of trimethoxyhexadecylsilane-coated Fe_3O_4 nanoparticles, J. Phys. Chem. C 21 (2010) 9802–9807.

35 J.A. Mikroyannidis Polyfluorenes containing tetraphenylthiophene segments: Synthesis, photophysics, and electroluminescence, J. Polym. Sci. Part A: Polym. Chem. 44 (2006) 4015.

36 S.J. Ren, R. Dawson, D.J. Adams, A.I. Cooper, Low band-gap benzothiadiazole conjugated microporous polymers, Polym. Chem. 4 (2013) 5585–5590.

37 T.M. Geng, D.K. Li, Z.M. Zhu, W.Y. Zhang, S.N. Ye, H. Zhu, Z.Q. Wang, Fluorescent conjugated microporous polymer based on perylene tetraanhydride bisimide for sensing o-nitrophenol, Anal. Chim. Acta 1011 (2018) 77–85.

38 C. Bleschke, J. Schmidt, D.S. Kundu, S.A. Blechert Thomas, A chiral microporous polymer network as asymmetric heterogeneous organocatalyst, Adv. Synth. Catal. 353 (2011) 3101–3106.

39 J.A. Mikroyannidis, I.K. Spiliopoulos, A.P. Kulkarni, S.A. Jenekhe, Synthesis and optical properties of poly (p-phenylenevinylene)s bearing tetraphenylthiophene or dibenzothiophene moieties along the main chain, Synthetic. Met. 142 (2004) 113–120.

40 L.X. Guo, Y.B. Xing, M. Wang, S. Ying, X.Q. Zhang, B.P. Lin, H. Yang, Luminescent liquid crystals bearing aggregation-induced emission active tetraphenylthiophene fluorophore, J. Mater. Chem. C 7 (2019) 4828–4837.

41 S. Dey, D.M. Esquivelb, C. Janiak, Covalent triazine-based frameworks (CTFs) from triptycene and fluorene motifs for CO_2 adsorption, J. Mater. Chem. A 4 (2016) 6259–6263.

42 S. Gu, J. He, Y. Zhu, Z. Wang, D. Chen, G. Yu, C. Pan, J. Guan, K. Tao, Facile carbonization of microporous organic polymers into hierarchically porous carbons targeted for effective CO2 uptake at low pressures, ACS appl. Mater. Inter. 8 (2016) 18383–18392.

43 C.T. Lai, R.H. Chien, S.W. Kuo, J.L. Hong, Tetraphenylthiophene-functionalized poly(N-isopropylacrylamide): Probing LCST with aggregation-induced emission, Macromolecules 44 (2011) 6546–6556.

44 N.N. Sang, C.X. Zhan, D.P. Cao, Highly sensitive and selective detection of 2,4,6-trinitrophenol using covalent-organic polymer luminescent probes, J. Mater. Chem. A 3 (2015) 92–96.

45 L. Guo, D.P. Cao, J. Yun, X.F. Zeng, Highly selective detection of picric acid from multicomponent mixtures of nitro explosives by using COP luminescent probe, Sensor. Actuat. B-Chem. 243 (2017) 753–760.

46 L. Guo, D.P. Cao, Color tunable porous organic polymer luminescent probes for selective sensing of metal ions and nitroaromatic explosives, J. Mater. Chem. C 3 (2015) 8490–8494.

47 L. Guo, X. Zeng, D. Cao, Porous covalent organic polymers as luminescent probes for highly selective sensing of Fe^{3+} and chloroform: Functional group effects, Sensor. Actuat. B-Chem. 226 (2016) 273–278.

48 J. Liu, K.K. Yee, K.K.W. Lo, K.Y. Zhang, W.P. To, C.M. Che, Z.T. Xu, Selective Ag(I) binding, H_2S sensing, and white-light emission from an easy-to-make porous conjugated polymer, J. Am. Chem. Soc. 136 (2014) 2818–2824.

49 P. Pallavi, S. Bandyopadhyay, J. Louis, A. Deshmukh, A. Patra, Soluble conjugated porous organic polymer: efficient white light emission in solution, nanoparticles. gel and transparent thin film, Chem. Commn. 53 (2017) 1257–1260.

View Article Online
DOI: 10.1039/D0NJ02912B

50 C. Gu, N. Huang, J. Gao, F. Xu, Y.H. Xu, D.L. Jiang, Controlled synthesis of conjugated microporous polymer films: Versatile platforms for highly sensitive and label-free chemo- and biosensing, Angew. Chem. 126 (2014) 4950–4955.

51 P. Zhang, J. Guo, C.C. Wang, CMP microspheres: multifunctional poly(phenylene ethynylene) frameworks with covalently built-in Fe_3O_4 nanocrystals exhibiting pronounced sensitivity for acetaminophen microdetection, J. Mater. Chem. 22 (2012) 21426–21433.

52 W. Zhang, L.G. Qiua, Y.P. Yuan, A.J. Xie, Y.H. Shen, J.F. Zhu, Microwave-assisted synthesis of highly fluorescent nanoparticles of a melamine-based porous covalent organic framework for trace-level detection of nitroaromatic explosives, J. Hazard. Mater. 222 (2012) 147–154.

53 N. Jiang, G.F. Li, W.L. Che, D.X. Zhu, Z.M. Su, R. Martin, Polyurethane derivatives for highly sensitive and selective fluorescent detection of 2,4,6-trinitrophenol (TNP), J. Mater. Chem. C 41 (2018) 11162–11169.

54 J.M. Yang, X.W. Hu, Y.X. Liu, W. Zhang, Fabrication of a carbon quantum dots-immobilized zirconium-based metal-organic framework composite fluorescence sensor for highly sensitive detection of 4-nitrophenol, Micropor. Mesopor. Mat. 274 (2019) 149–154.

55 Y.K. Li, S.M. Bi, F. Liu, S.Y. Wu, J. Hu, L.M. Wang, H.L. Liu, Y. Hu, Porosity-induced emission: exploring color-controllable fluorescence of porous organic polymers and their chemical sensing applications, J. Mater. Chem. C 3 (2015) 6876–6881.

56 C. Gu, N. Huang, Y. Wu, H. Xu, D.L. Jiang, Design of highly photofunctional porous polymer films with controlled thickness and prominent microporosity, Angew. Chem. Int. Ed. 54 (2015) 11540–11544.

57 L.L. Zhang, T.T. Lin, X.Y. Pan, W.Z. Wang, T.X. Liu, Morphology-controlled synthesis of porous polymer nanospheres for gas absorption and bioimaging applications, J. Mater. Chem. 22 (2012) 9861–9869.

58 G. Das, B.P. Biswal, S. Kandambeth, V. Venkatesh, G. Kaur, M. Addicoat, T. Heine, S. Verma, R. Banerjee, Chemical sensing in two dimensional porous covalent organic nanosheets, Chem. Sci. 6 (2015) 3931–3939.

59 Y.W. Zhang, A. Sigen, Y.C. Zou, X.L. Luo, Z.P. Li, H. Xia, X.M. Liu, Y. Mu, Gas uptake, molecular sensing and organocatalytic performances of a multifunctional carbazole-based conjugated microporous polymer, J. Mater. Chem. A 2 (2014) 13422–13430.

60 D.X. Wang, S.Y. Feng, H.Z. Liu, Fluorescence-tuned polyhedral oligomeric silsesquioxane-based porous polymers, Chem. Eur. J. 22 (2016) 14319–14327.

61 G.Q. Lin, H.M. Ding, D.Q. Yuan, B.S. Wang, C. Wang, A pyrene-based, fluorescent three-dimensional covalent organic framework, J. Am. Chem. Soc. 138 (2016) 3302–3305.

62 D.H. Zhao, T.M. Swager, Sensory responses in solution vs solid state: A fluorescence quenching study of poly(iptycenebutadiynylene)s, Macromolecules 38 (2005) 9377–9384.

63 G. He, H. Peng, T. Liu, M. Yang, Y. Zhang, Y. Fang, A novel picric acid film sensor via combination of the surface enrichment effect of chitosan films and the aggregation-induced mission effect of siloles, J. Mater. Chem. 19 (2009) 7347–7453.

64 W.B. Wu, S.H. Ye, G. Yu, Y.Q. Liu, J.G. Qin, Z. Li, Novel functional conjugative hyperbranched polymers with aggregation-induced emission: synthesis through one-pot “A2+B4” polymerization and application as explosive chemsensors and PLEDs, Macromol. Rapid Commun. 33 (2012) 164–171.

65 J. Ma, L. Bian, L. Zhao, X.T. Feng, L.Z. Zhao, Z.Y. Wang, Q.S. Pu, Dialysed caramel as an effective fluorophore for the simultaneous detection of three nitrophenols, Talanta 197 (2019) 159–167.

View Article Online
DOI: 10.1039/D0NJ02912B

Graphical Abstract